Food Packaging and Shelf Life 52 (2025) 101644

Contents lists available at ScienceDirect

Food Packaging and Shelf Life

journal homepage: www.elsevier.com/locate/fpsl

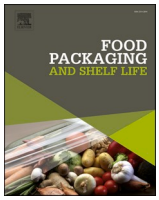

Analysis of protective ability of pomelo peel against impact damage to apple for cushioning packaging design

Jincheng Yu [a], Hongli Qiang [a], Wenzhi Tang [b], Fideline Tchuenbou-Magaia [c], Fauconnier Marie-Laure [d], Clément Burgeon [d], Minggang Wang [a], Yande Liu [e], Zhiguo Li [a,*]

[a] College of Mechanical and Electronic Engineering, Northwest A&F University, Yangling, Shaanxi 712100, China
[b] College of Food Science and Engineering, Northwest A&F University, Yangling, Shaanxi 712100, China
[c] School of Engineering, Computing and Mathematical Sciences, University of Wolverhampton, Wolverhampton WV1 1LY, UK
[d] Laboratory of Chemistry of Natural Molecules, University of Liège, Liège 7B-4000, Belgium
[e] School of Mechatronics & Vehicle Engineering, East China Jiaotong University, Nanchang 330000, China

ARTICLE INFO

Keywords:
Fresh fruit
Mechanical damage
Microstructure
Bionic model
Packaging material

ABSTRACT

The design of high-performance cushioning structures plays a crucial role in preventing mechanical damage to apples during storage, handling and transportation. The impact test, microstructure observation and discrete element method were employed to assess the protective effect of pomelo peel on the damage resistance of apples. The results showed that the 'Red honey' pomelo peel was more suitable as a packaging material than the 'Shatian' pomelo peel due to its thinner structure and comparable strain resistance. The mesocarp of the 'Red Honey' pomelo exhibits a distinct reticular structure despite its reduced thickness. This architecture allows the peel to tolerate higher impact force (116.53 N) and elastic modulus (1.10 MPa), indicating that protective performance is governed by structural design rather than tissue bulk. Based on the cell structure and intercellular pore size characteristics of the pomelo mesocarp, a biological damage-resistant structure prediction model was developed. The results demonstrated that the predictive mathematical model exhibited a good fit (R^2= 0.9003), with pomelo peel impact resistance prediction of 0.1766 ms. The factors influencing the damage resistance of the model's structural blocks followed the order: loading velocity (V) > porosity (P) > block size (S). Pomelo peel offers a structural model for protective produce packaging.

1. Introduction

Apples represent one of the most widely consumed fruit crops globally, valued for their high nutritional content and palatability. They play a significant role in the agricultural economies of many nations, with an estimated global production of approximately 84 million metric tons. China leads apple production with around 48 million metric tons every year, followed by the European Union (11.01 million metric tons), the United States (4.89 million metric tons), and Turkey (4.15 million metric tons) (https://www.fas.usda.gov/data/production?commodity=apples). However, their delicate skin and sensitive flesh make them highly susceptible to mechanical damage during storage and transportation, resulting in fruit deterioration and nutrient loss (Al-Dairi et al., 2021). Studies have shown that approximately 80 % of fruit losses occur during transportation (Jiao et al., 2021). In the context of express logistics, mechanical damage to fruit often arises from friction, collisions, and other interactions between the fruit and packaging structures (Yu et al., 2024). In our previous study, we found that the damage rate of apples during express transportation ranged from 9.09 % to 63.64 % (Keyhan et al., 2024; Yu et al., 2025). Throughout the shipping process, repeated compression, impacts, and friction forces exerted on the internal packaging materials can progressively weaken their structural integrity (Xu et al., 2024; dos Santos Lima et al., 2024)). This reduction in strength and subsequent plastic deformation ultimately diminishes the packaging's ability to protect the fruit (Al-Dairi et al., 2022). Macroscopic failure of packaging materials typically occurs when the applied stress exceeds the material's yield strength or fracture strength (Pisani et al., 2022). On a microscopic level, failure may result from alterations in the material's crystalline structure, leading to a decline in its mechanical properties (Wang et al., 2022). These failure mechanisms are closely related to the distribution of compressive, impact, and vibrational forces experienced by the packaging structure

* Corresponding author.
E-mail address: lizhiguo0821@163.com (Z. Li).

https://doi.org/10.1016/j.fpsl.2025.101644
Received 16 July 2025; Received in revised form 6 October 2025; Accepted 8 October 2025
Available online 13 October 2025

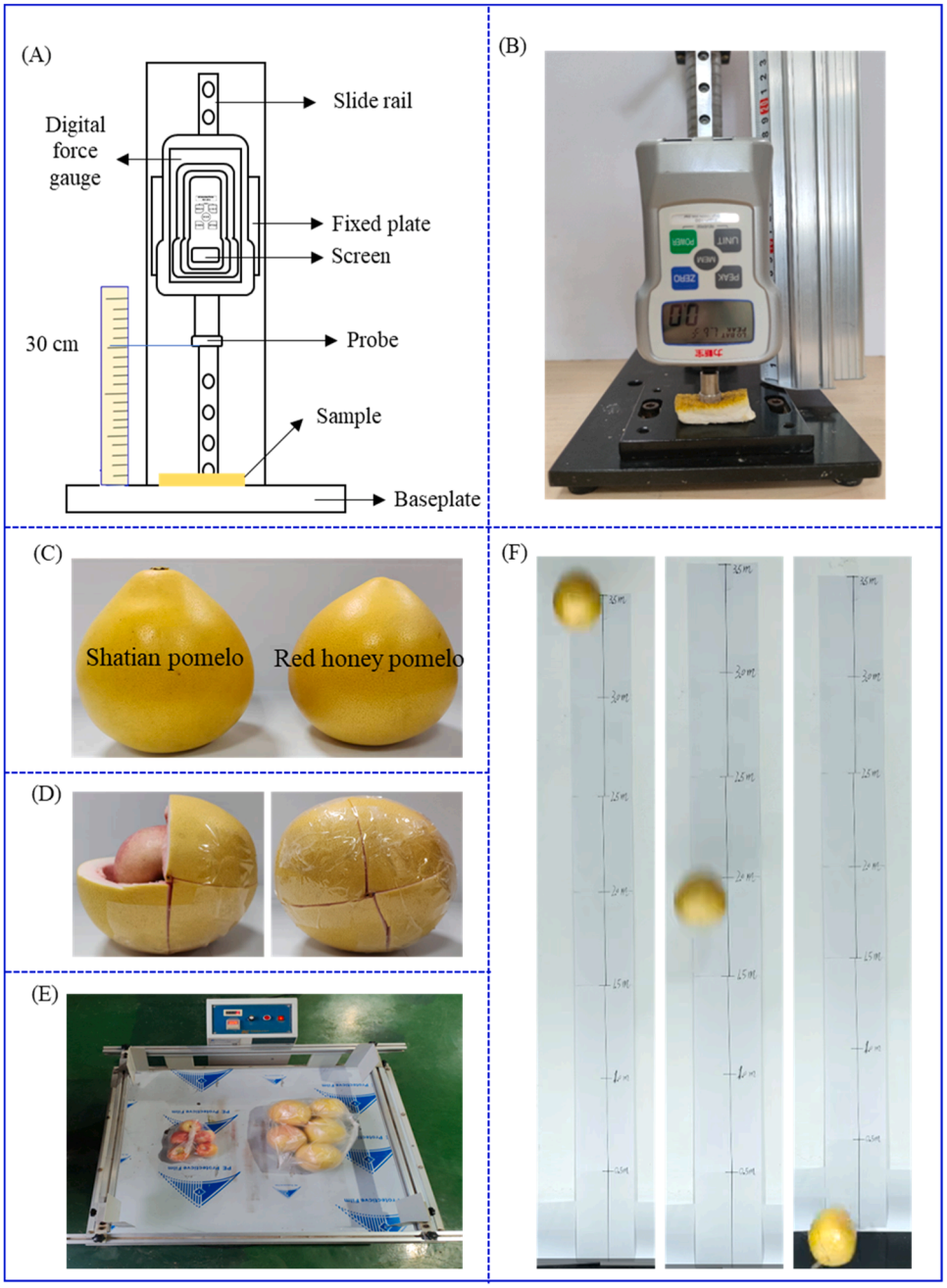

Fig. 1. Experimental setup and procedures for evaluating pomelo peel-inspired fruit packaging. (A) Schematic diagram of the designed sliding-rail impact testing device; (B) Photograph of the actual impact tester; (C) Images of two pomelo cultivars: Shatian pomelo and Red honey pomelo; (D) Preparation of apple packaging using pomelo peel; (E) Apples and pomelo peel-wrapped apples placed on a vibration testing platform; (F) Free-fall impact tests of pomelo peel-wrapped apples from different heights.

during transit (Zhu et al., 2024).

In the field of packaging structure research, Chen (2022) developed a vibration-damping packaging box for 'Hongmeiren' mandarins by designing a collapsible plastic crate as the outer packaging. The crate was divided into two layers using polypropylene (PP) sheets, with each layer featuring a rigid plastic partition that created 24 individual compartments for fruit placement, totaling 48 compartments. This design was tested under simulated express logistics conditions at 20 °C and 90 % relative humidity (RH) for 3 h. Results showed that the damage rate of mandarins in the compartmentalized packaging was 5.56 %, which was 80 % lower than that of mandarins packed without internal partitions. Shirzad and Joodaky (2023) investigated the impact of circular hole size and positioning on the buckling strength of corrugated cardboard. Their findings indicated that larger circular holes reduced the board's buckling strength, whereas holes positioned closer to the horizontal edge improved buckling resistance. Garbowski et al. (2021) demonstrated that increasing the basis weight of cardboard improved box strength. Moreover, when the openings were smaller and located near the center of the panel, the overall strength of the box was enhanced. Zhou et al. (2023) introduced a novel fiberboard structure that replaced the traditional three-layer corrugated design with an accordion-style isosceles trapezoidal structure. This innovative design exhibited a compressive strength of 0.853 MPa, surpassing the 0.735 MPa achieved by conventional fiberboard. Furthermore, the new fiberboard's elastic strength was approximately 35 % higher than that of traditional designs. Chaiwong et al. (2023) explored the use of natural

rubber latex foam nets (NRL-FN) reinforced with bamboo leaf fiber (BLF) for guava fruit packaging. Their results indicated that NRL-FN reduced vibration-induced bruising to less than 2.5 % of the fruit's surface area. Notably, NRL-FN with a lower BLF content (2.5 %) exhibited superior cushioning performance, reducing bruising by approximately 42.5 % compared to unpackaged guavas. The NRL-FN's performance was statistically comparable to that of commercial expanded polyethylene foam nets (EPE-FN). An et al. (2023) investigated the effect of expanded polyethylene (EPE) foam net thickness on strawberry damage. Their findings showed that for every 1 mm increase in EPE net diameter, the bruised volume and bruised volume percentage decreased by 33.7132 mm^3 and 0.1814 %, respectively. Despite these advances, most existing studies focus on macroscopic packaging designs or materials for specific fruit types under limited testing conditions. Few investigations consider the fruit's intrinsic microstructure, such as the cellular architecture and intercellular spaces, which play a critical role in impact resistance, which forms the basis of the present study.

In natural evolution, many plant fruit have developed unique morphological and physiological structures that exhibit remarkable mechanical performance allowing them to adapt and resist stresses such as those encountering during transit (Kishore et al., 2024). Inspired by these natural designs, various biological protective packaging materials have been employed to prevent fruit damage during storage and transportation. Among these, pomelo peel stands out by its distinct multilayered architecture, consisting of the exocarp, mesocarp, and endocarp. The exocarp consists of densely packed cells containing waxy or oily substances, providing a protective outer barrier. The mesocarp, the thickest layer of the peel, features a soft, sponge-like structure composed of numerous pores and large cellular gaps. The endocarp is directly adjacent to the fruit pulp and is characterized by loosely arranged cells. This unique multilayer structure enables the pomelo peel to effectively mitigate mechanical stresses. When subjected to external forces, the exocarp offers structural support to minimize deformation, while the highly porous, sponge-like mesocarp converts compressive, impact, or vibrational forces into fiber deformation, effectively dissipating strain energy and preserving the fruit's integrity (Yang et al., 2022b). Due to its exceptional impact energy dissipation capabilities, the pomelo peel structure has become an ideal model for developing biomimetic impact-damping materials (Gu et al., 2024). Hu et al. (2024) retained the three-dimensional structure of pomelo peel through chemical treatments and combined it with polyacrylamide hydrogel via hydrogen bonding to fabricate a pomelo peel-based hydrogel. This biomimetic structure, composed of microfibrous absorbent cotton and nanofibrous chitin, demonstrated impressive softness and elasticity, exhibiting only a 12.25 % irreversible strain after 5000 compression cycles. In another study, Schäfer et al. (2020) employed finite element modeling to construct a biomimetic foam model inspired by pomelo peel. The results showed that when the internal porosity of the foam's supporting pillars was 10 %, the maximum compressive strength reached 125 MPa. Additionally, Yang et al. (2022b) synthesized a composite hydrogel by in situ polymerizing polyacrylamide within the 3D network of delignified pomelo peel. Remarkably, the composite hydrogel achieved approximately 2.5 times the compressive strength of conventional polyacrylamide hydrogel despite the pomelo peel hydrogel accounting for only 1.3 % of the total mass.

Significant progress has been made by researchers worldwide in understanding the relationship between vibration-damping packaging and mechanical damage to fruit and vegetables, developing cushioning packaging materials, and designing pomelo peel-inspired packaging structures using finite element analysis (An et al., 2023; Hu et al., 2024; Yang et al., 2022a). In the field of biological pomelo peel packaging material development, most studies have focused on chemically fabricating materials that mimic the structural characteristics of the pomelo mesocarp, or constructing simplified and homogeneous pomelo peel structure models via finite element methods to investigate their compressive properties. However, in real-world scenarios, the failure of packaging materials during transport is rarely attributed to the breakdown of a single structure; instead, it often results from the combined effects of multiple interacting structural components. Fresh pomelo peel was selected as the cushioning material because of its unique structural and mechanical characteristics. Fresh pomelo peel exhibits a natural reticulated porous architecture with intercellular spaces that provide excellent flexibility, resilience, and structural integrity. These features allow the peel to absorb and dissipate impact energy effectively, thereby reducing mechanical damage to the packaged fruit. Despite these promising insights, there remains a notable gap in research regarding the quantitative characterization of pomelo mesocarp cellular structures and pore dimensions for modeling purposes. Such detailed modeling is essential for developing biological packaging materials that can better withstand mechanical stresses during fruit transportation. Therefore, this study aims to address this gap by employing a discrete element model (DEM) to evaluate the damage resistance performance of pomelo mesocarp-inspired packaging structures.

2. Materials and methods

2.1. Determination of damage prevention ability and microstructure characteristics of pomelo peel

2.1.1. Design of impact test bed falling along slide rail

As illustrated in Fig. 1A, the force measurement apparatus primarily consists of a digital force gauge (Model: FGP-100; maximum measuring force: 1000 N; accuracy 0.1 N), a sliding block, a slide rail, and a fixed plate. The intermediate connecting plate, digital force gauge, and sliding block were securely fastened together using bolts to form an integrated movable unit. This integrated unit was then mounted onto the fixed plate to ensure stability during testing. To measure the impact force at different heights, the sliding block's position was adjusted without moving the entire apparatus. After turning on the digital force gauge by pressing the "Power" button, the gauge was positioned 30 cm above a rigid surface and released to fall freely along the slide rail, striking the pomelo peel sample below it. Upon impact, the force gauge automatically recorded the maximum impact force during the drop. The peak force value was displayed by pressing the "Peak" button on the gauge screen.

2.1.2. Determination of impact damage resistance of pomelo peel

Five fresh, undamaged pomelos from each of the two varieties, 'Shatian' pomelo (*Citrus maxima cv*. Shatianyou) and 'Red honey' pomelo (*Citrus maxima cv*. Hongxinmiyou) (Fig. 1C), were selected for the experiment. Pomelos with weight of 1.2–1.5 kg and 80 % maturity ('Red honey' pomelo: yellow peel with slight green coloration and soluble solids content of 10–11 °Brix; 'Shatian' pomelo: yellow-green peel, firm mesocarp texture, and a soluble solids content of 9–10 °Brix) were purchased from local supermarket (latitude 34.17 °N, longitude 108.04 °E). All fruit samples were sourced from the same batch. All samples were stored at 20 ± 1 °C and 60–70 % relative humidity for no more than 24 h before testing to preserve freshness and minimize moisture variation in the peel. To remove surface dust and other debris, the fruit peels were wiped clean using a damp paper towel. Each pomelo was then cut along its equatorial direction into rectangular pieces measuring 40 × 25 mm. The prepared pomelo peel samples were placed on the fixed plate at the bottom of the impact testing device (Fig. 1B). The inner layer of the peel was positioned facing the fixed plate, while the outer layer faced the impact probe of the force gauge. This placement was designed to simulate the protective role of the pomelo peel in resisting sudden external impacts when surrounding the fruit pulp. After turning on the digital force gauge by pressing the "Power" button, the gauge was positioned 30 cm above a rigid surface and released to fall freely along the slide rail, striking the surface of the pomelo peel sample. The force gauge automatically recorded the peak impact force during the drop.

2.1.3. Mechanical properties of pomelo pericarp

A fresh pomelo was carefully cut open using a sharp fruit knife, and the pulp was completely removed, leaving only the peel. To ensure consistent sample dimensions for mechanical testing, the outer and inner layers of the pomelo peel were carefully trimmed away, retaining only the middle layer. The middle peel was then cut into rectangular samples with a length-to-width ratio of 6:1. For uniformity across all test samples, each specimen was further trimmed to standardized dimensions of 4 × 24 mm. The prepared middle peel samples were securely clamped between the upper and lower plates of a texture analyzer (Universal TA, Shanghai Tengba Instrument Technology Co., Ltd., China). The initial gap between the upper and lower tensile fixtures was set to 20 mm, and the tensile speed was maintained at 1 mm s^{-1}. After configuring the testing parameters, the tensile test was conducted, with the computer recording the force-displacement data in real time throughout the experiment. The mechanical properties of the pomelo peel, including fracture stress (σy), fracture strain (εy), and elastic modulus (E), were calculated by Eqs. (1), (2), and (3) (Yang et al., 2024).

$$\sigma_y = \frac{F_{max}}{A} \tag{1}$$

$$\varepsilon_y = \frac{\Delta L}{L} \tag{2}$$

$$E = \frac{\sigma_y}{\varepsilon_y} \tag{3}$$

where, σ_y - fracture stress, MPa; F_{max} - elastic peak force, N; A - cross-sectional area, mm^2; ε_y - fracture strain, -; ΔL - change in sample length before and after test, mm; L - initial length of sample, mm; E - modulus of elasticity, MPa.

2.1.4. Microstructure characterization of pomelo peel

(1) Observation of pomelo peel structure using safranin-fast green staining method

Pomelo peel samples were cut into approximately 0.5 cm^3 cubes using an R35 blade. The tissue samples were fixed in a 5 % formalin-acetic acid-ethanol (FAA) solution for 48 h. Following fixation, the samples were embedded in paraffin. The embedded pomelo peel samples were sectioned into 2 μm-thick slices using a microtome (RM2016, Leica Instruments Co., Ltd., Shanghai, China). The prepared sections were stained in safranin dye for 1.5 h, followed by an 8 s differentiation step in ethanol. The sections were then immersed in a fast green stain for 60 s and subsequently treated with absolute ethanol and xylene for 5 min each. Finally, the stained sections were examined, and their morphological characteristics were captured using a microscope (CI-S, Nikon, Japan) (Chen et al., 2021).

(2) The pomelo peel structure was observed by electron microscope

Using a sharp blade, the pomelo peel samples prepared in Section 2.1.2 were cut into 2 mm pieces then placed in a clean Petri dish. The Petri dish containing the samples was promptly placed at the center of an XY-axis precision stage, which had been pre-fixed above the light source of a Phenix XTL-165-VT stereomicroscope (Phenix Optical Co., Ltd., China). To capture the entire upper surface (equatorial cross-section) of the pomelo peel samples, the X-axis knob was rotated to move the stage left and right, while the Y-axis knob was adjusted to move the stage forward and backward. The microscopic features of the sample surface were continuously recorded using an MC-D500U/TP digital camera module (Liu et al., 2020).

(3) Extraction and scanning electron microscopy (SEM) observation of pomelo mesocarp fiber structure

Extraction of pomelo mesocarp fiber structure: Fresh pomelo mesocarp from 'Red honey' pomelo was cut into 2 × 2 mm block samples using a sharp blade. The prepared mesocarp samples were placed in a beaker, and a 2 % sodium hypochlorite solution was adjusted to pH 4.6 using hydrochloric acid. This solution was then added to the beaker containing the pomelo mesocarp samples. The mixture was subjected to an oil bath at 100 °C for 6 h to remove lignin. Following the oil bath treatment, the samples were immersed in a solution of deionized water and industrial ethanol (1:1 v/v) to wash away residual sodium hypochlorite and other chemicals. Next, the samples were soaked in an 8 % sodium hydroxide (NaOH) solution and subjected to an oil bath at 80 °C for 8 h to remove hemicellulose. Afterward, the samples were transferred to a deionized water and ethanol solution (1:1 v/v) to eliminate excess NaOH and other residues. The cleaned samples were then centrifuged at 10742 g for 10 min. The resulting residue was dried in a 30 °C oven to remove any remaining moisture, yielding pomelo mesocarp fiber powder (Gao et al., 2023).

Scanning electron microscopy (SEM) (TM3000, Hitachi, Japan) observation of pomelo mesocarp fiber structure: The obtained pomelo mesocarp fiber powder was affixed to a circular SEM sample stage using conductive adhesive tape. The sample was then placed in a vacuum sputter coater and coated with gold at 1 mA for 10 min. After sputter coating, the prepared sample was transferred to the SEM vacuum chamber. Image brightness, magnification, and other parameters were adjusted to capture clear images of the fiber structure using the scanning electron microscope.

2.2. Assessment of apple impact resistance using pomelo peel wrapping

To evaluate the impact resistance of apples wrapped in pomelo peel, five fresh apples and five fresh pomelos of uniform size, shape, and without mechanical damage were selected. Prior to wrapping, the weight of each apple (m) was recorded. The fresh pomelos were peeled, and the separated pomelo peels were used to wrap the apples. Transparent adhesive tape was employed to secure the peel around each apple (Fig. 1D). Once wrapped, the samples were subjected to free-fall drop tests from a consistent height onto a hard, rigid surface (Fig. 1F). Additionally, five unwrapped apples were tested under identical conditions as a control group (An et al., 2022). Both the wrapped and unwrapped apples were positioned at a fixed height above the rigid surface. The drop height at which visible damage occurred was recorded. The instantaneous velocity (v), impact energy (P), and maximum impact force (F) upon contact with the rigid surface were calculated using Eqs. (4), (5), and (6), respectively. The impact energy (P) was used as the primary indicator of the apple's resistance to impact-induced damage.

$$v^2 = 2gh \tag{4}$$

$$P = mv \tag{5}$$

$$F = mg \tag{6}$$

where, v - instantaneous velocity, m s^{-1}; g - acceleration of gravity, 9.8 m s^{-2}; h - drop height, m; P - impact energy, kg m s^{-1}; F - impact force, N.

2.3. Assessment of apple resistance to vibration-induced damage with pomelo peel wrapping

To evaluate the vibration resistance of apples wrapped in pomelo peel, 20 wrapped apples were evenly distributed into four PET bags, with five apples in each bag. One of these bags served as the control group and was not subjected to vibration testing. The remaining three bags were individually placed on a vibration test platform (Qingdao Rongle Technology Information Service Co., Ltd., Qingdao, China) and subjected to continuous vibration at a frequency of 3.5 Hz for 2 h (Dagdelen and Aday, 2021; Zhang et al., 2023). In addition, an electronic apple (7602A8, Martin Lishman Ltd, UK) was wrapped in pomelo peel and used to measure the maximum acceleration (a_{max}) experienced during vibration (Fig. 1E). Following the vibration test, the apples were

Table 1
Cell and intercellular pore size of pericarp in pomelo.

No.	Major axis (mm)	Minor axis 1 (mm)	Minor axis 2 (mm)
1	0.14	0.14	0.14
2	0.14	0.06	0.06
3	0.14	0.03	0.03
4	0.07	0.14	0.14
5	0.07	0.06	0.06
6	0.07	0.03	0.03
7	0.03	0.14	0.14
8	0.03	0.06	0.06
9	0.03	0.03	0.03
j1	0.35	0.33	0.33
j2	0.35	0.16	0.16
j3	0.19	0.33	0.33
j4	0.19	0.16	0.16
j5	0.19	0.07	0.07
j6	0.08	0.33	0.33
j7	0.08	0.16	0.16

Note: In the table, 1–9 indicates the cell size, and j1-j7 indicates the size of the intercellular pores.

immediately inspected for damage, and the maximum impact force (F_{max}) was calculated using Eq. (7). The maximum impact force experienced during vibration was used as the key indicator of the apples' resistance to vibration-induced damage.

$$F_{max} = ma_{max} \tag{7}$$

where, F_{max} - the maximum vibration force of apple, N; m - apple mass, kg; a_{max} - the maximum acceleration experienced by the apple during vibration, g.

2.4. Establishment of a bionic model for pomelo mesocarp tissue blocks and evaluation of its damage resistance performance

2.4.1. Measurement of pomelo mesocarp cell and intercellular pore dimensions

A micrometer (range: 1 mm; precision: 0.01 mm) was placed at the center of the microscope stage. The microscope's focus knob was adjusted to ensure the micrometer scale was aligned with the center of the microscope's field of view and clearly visible. Images of the pomelo peel structure obtained from Section 2.1.4 were imported into the image analysis software "Phenix". The software's calibration function was used to set the measurement scale, with the micrometer scale serving as the reference standard. The dimensions of the pomelo mesocarp cells and intercellular pores were measured using this calibrated scale. For each cell and intercellular pore, the major and minor axes were identified and measured. The major axis was defined as the longest diameter passing through the center of the cell or pore, while the minor axis 1 was defined as the shortest diameter in the same plane. Additionally, the side view's minor axis (minor axis 2) was considered equivalent to minor axis 1, i.e., minor axis 1 = minor axis 2 (Zhang et al., 2022). The measured dimensions of pomelo mesocarp cells and intercellular pores are presented in Table 1.

2.4.2. Establishment of a composite tissue block model for pomelo mesocarp cells and intercellular pores

First, based on the dimensional parameters of pomelo mesocarp cells and intercellular pores obtained in Section 2.4.1, several independent models of pomelo mesocarp cells and intercellular pores were constructed using SolidWorks software (2022, Dassault Systèmes Americas Corp., USA). These independent models were then imported into EDEM software (2022, Dassault Systèmes Americas Corp., USA). Within EDEM, suitable solid particles were selected from the software's particle shape library to automatically calculate and fill the independent models. The filled particle shapes were required to match the dimensions and geometry of the imported models. If discrepancies occurred, adjustments were made by modifying the particle radius and spatial coordinates to improve the fit between the particles and the original models. The density, elastic modulus, and Poisson's ratio of the cell and intercellular pore models were defined as 1.265 g cm^{-3} , 900 MPa, and 0.28, respectively (Yang et al., 2022a). Next, a cubic box (3 mm × 3 mm × 3 mm) was created in the software to generate the composite pomelo mesocarp tissue block model. The box size was adjustable to accommodate varying experimental parameters and was designed to aggregate and form a square block composed of multi-sized particles. A static virtual square (3 mm × 3 mm) was created on the upper plane of the cubic box and designated as the particle generator. The particle generation time was set to 0.0002 s. To simulate the interactions between adjacent cells and intercellular pore particles within the composite tissue block model, the static friction coefficient and dynamic friction coefficient were set to 0.3 (Yang et al., 2022a). The Hertz-Mindlin with Bonding contact model was employed to define bonding interactions between neighboring cell particles, representing the cohesive behavior of the pomelo mesocarp tissue block structure (Shaikh et al., 2021).

Table 2
Test factors and their respective levels.

Factors	Level		
S: Size/mm^3	3	4	5
P: Poriness /%	25	35	45
V: Velocity / m s^{-1}	2	4	6

2.4.3. Impact resistance analysis of the composite model of pomelo mesocarp cells and intercellular pores

A cylindrical object with a diameter of 0.6 mm was created on the upper plane of the established 3D pomelo mesocarp model to simulate vertical downward motion. The total operation time of the cylinder was set to 0.001 s, and the initial height between the cylinder and the tissue block model was defined as 0.3 mm. During the simulation, the cylinder was allowed to fall freely under gravitational acceleration (9.8 m s^{-2}). After completing the setup, the simulation was initiated to analyze the impact resistance of the model. From the simulation results, the impact force-time relationship data were extracted. The model's impact resistance capability was represented by the time span (Δt) from the moment the cylinder contacted the tissue block model to the moment the tissue block experienced the maximum force. A Box-Behnken central composite design in Design-Expert software was employed to design the experiment, with size, porosity, and velocity as the investigated factors. The experimental factor design table is shown in Table 2.

2.5. Data analysis

Analysis of variance and regression were performed using Design-Expert software, version 22.0 (IBM Inc., Chicago, IL, USA). Using Origin software, 2018 version (Origin Laboratories, Ltd., Northampton City, MA, USA) and GraphPad Prism software, Version 9.0 (GraphPad software Inc., San Diego, CA, USA) graphing.

3. Results and discussion

3.1. Analysis of impact damage resistance of pomelo peel

Fig. 2 illustrated the impact resistance capabilities of 'Shatian' pomelo and 'Red honey' pomelo peels. The peel thickness was measured before and after impact testing. As shown in Fig. 2A, the average peel thicknesses of 'Shatian' pomelo and 'Red honey' pomelo before impact were 9.55 mm and 3.97 mm, respectively. After impact, their average peel thickness was reduced to 2.26 mm and 1.34 mm, respectively, with a significant difference observed between the two varieties post-impact. The maximum force recorded by the force gauge during its drop onto the pomelo peels was defined as the indicator of impact resistance. The

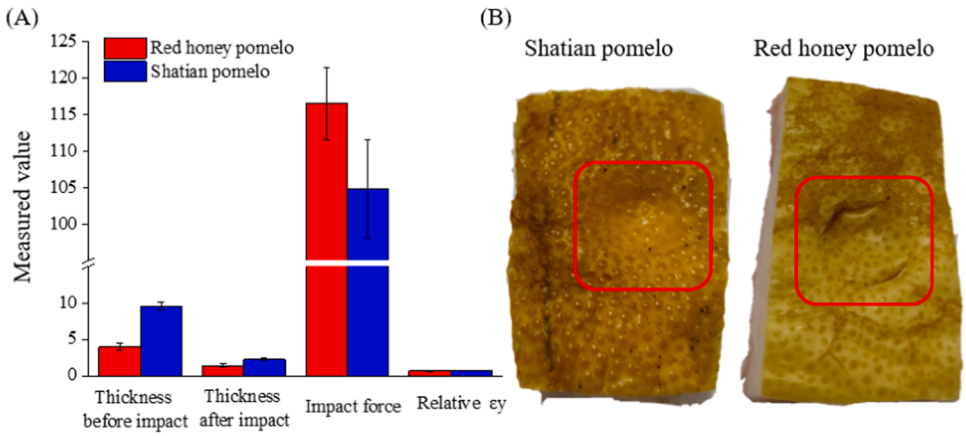

Fig. 2. The impact damage resistance of 'Shatian' pomelo and 'Red honey' pomelo peel. (A): Mechanical parameters of two kinds of pomelo peel after impact, thickness (mm), impact force (N), and εy (-); (B): Surface damage patterns of two kinds of pomelo peel after impact.

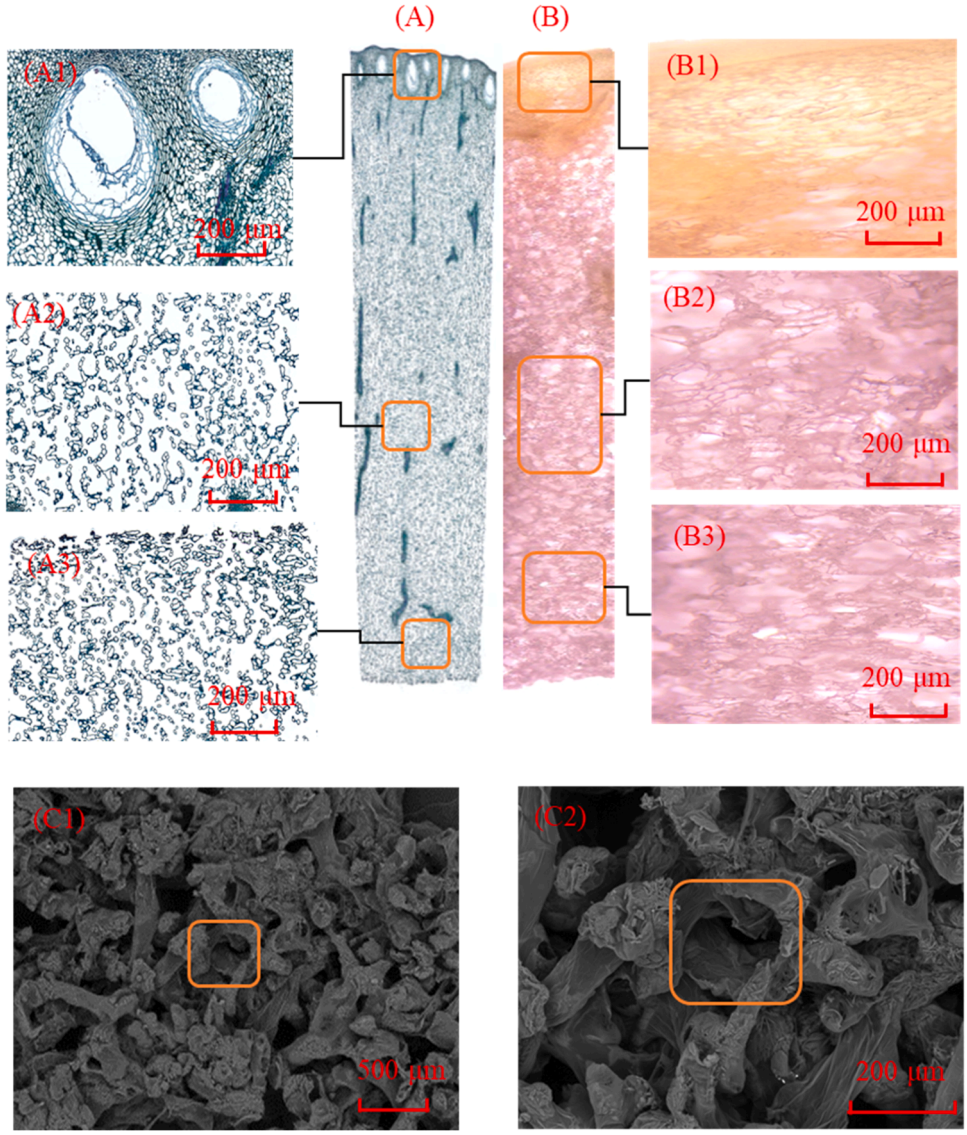

Fig. 3. Microstructure of pomelo peel at different magnifications. (A): Scanned images of pomelo peel cross-sections after safranin-fast green staining; (B): Microstructural images of pomelo peel observed under scale bars of 200 μm; (C): SEM images of delignified and hemicellulose-removed middle pomelo peel with scale bars of 500 μm and 200 μm.

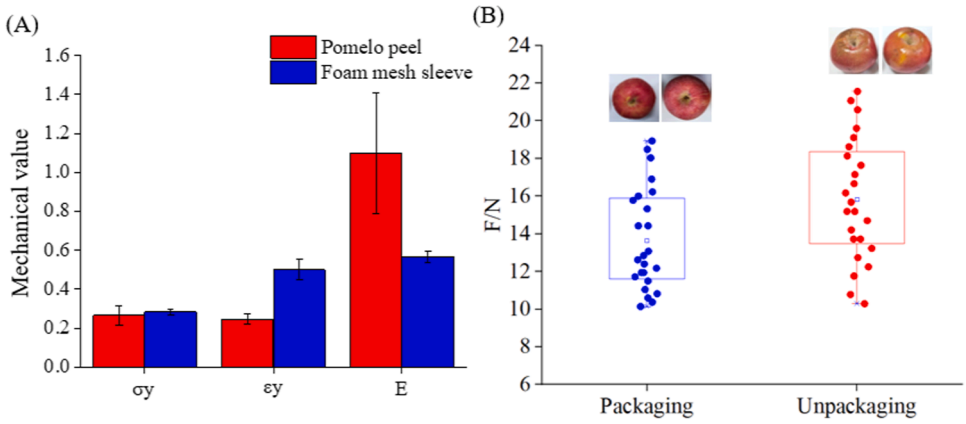

Fig. 4. Mechanical properties of 'Red honey' pomelo peel and vibration resistance of apples wrapped in pomelo peel. (A): Mechanical properties of 'Red honey' pomelo peel, σy (MPa), εy (-), and E (MPa) represent stress, strain, and elastic modulus, respectively; (B): Vibration resistance of apples wrapped in pomelo peel.

maximum impact forces for 'Shatian' pomelo and 'Red honey' pomelo peels were 104.87 N and 116.53 N, respectively. These results indicate that, under the same drop height, the 'Shatian' pomelo peel experienced less impact force compared to the 'Red honey' pomelo peel. The relative strain values for 'Shatian' pomelo and 'Red honey' pomelo peels were 0.76 and 0.66, respectively. This suggests that the 'Red honey' pomelo peel exhibits superior energy dissipation characteristics, ductility, and flexibility under impact stress (Jentzsch et al., 2022). From the post-impact surface damage morphology shown in Fig. 2B, the 'Shatian' pomelo peel exhibited less visible damage compared to the 'Red honey' pomelo peel. This may be attributed to the greater thickness of the 'Shatian' pomelo peel, as thicker peels are generally more effective in dispersing impact forces (Thielen et al., 2013). These findings suggest that 'Shatian' pomelo peels primarily rely on their thickness to dissipate impact forces, while 'Red honey' pomelo peels utilize elastic deformation for energy absorption. The superior flexibility of 'Red honey' pomelo peels offers an advantage in environments requiring deformation and recovery. Consequently, for applications involving complex shipping and handling conditions, 'Red honey' pomelo peels may be a more suitable material for subsequent studies.

3.2. Microstructure of 'Red honey' pomelo peel

Fig. 3 presented the microscopic images of pomelo peel observed under different magnifications. As shown in Figure 3A1, at a scale of 200 μm, the cells located near the oil glands in the outer peel are elliptical in shape and tightly packed. Moving farther from the oil glands, the peel cells gradually transition from an elliptical to a more circular shape, with a noticeable decrease in cell packing density. As depicted in Figures 3A2 and 3A3, both mesocarp and inner peel cells exhibit irregular elliptical shapes with relatively loose arrangements, characterized by numerous intercellular pore structures. The mesocarp cell arrangement is less compact compared to the inner peel cell arrangement. Under scale bars of 200 μm with electron microscope Figure 3B1 illustrates that the outer peel cells exhibit a distinctly denser structure. In contrast, Figures 3B2 and 3B3 showed that mesocarp and inner peel cells display a more open, reticulated arrangement, with the mesocarp structure being less compact than that of the inner peel. Following chemical treatments to remove lignin and hemicellulose, Figures 3C1 and 3C2 revealed that the mesocarp cell arrangement adopts a more intricate reticulated structure, with more pronounced size variations in the intercellular pores. The strong interfacial interactions induced by hydrogen bonding enable the mesocarp and outer peel layers to bond tightly together, providing a protective barrier that helps mitigate mechanical damage to the fruit pulp (Feng et al., 2025). Additionally, the removal of lignin and hemicellulose further exposes the porous structure between mesocarp cells, resulting in a highly porous, loose network that effectively absorbs impact energy (Lazarus et al., 2023). In combination with the impact resistance and strain performance of 'Red honey' pomelo peel, a dense outer epidermis and a porous of 'Red honey' pomelo peel, reticulated mesocarp synergistically confer both stiffness and energy dissipation capacity. Despite its reduced thickness, the peel exhibits higher impact force tolerance and elastic modulus, suggesting that its internal architecture, rather than bulk alone, governs its macroscopic protective performance. This structure–function integration underscores the peel's potential as a lightweight, deformable, and biodegradable material for next-generation bioinspired packaging.

3.3. The ability to resist vibration damage of the apple wrapped in the peel of the 'Red honey' pomelo

As shown in Fig. 4A, the mechanical properties of two protective materials—pomelo peel and foam mesh sleeve—were compared in terms of stress (σy), strain (εy), and elastic modulus (E). For the 'Red Honey' pomelo peel, the measured values were 0.27 MPa for σy, 0.25 for εy, and 1.10 MPa for E. In contrast, the foam mesh sleeve exhibited a σy of 0.28 MPa, an εy of 0.50, and an E of 0.57 MPa. While the yield stress values of the two materials were comparable, the pomelo peel demonstrated a significantly higher elastic modulus, indicating superior stiffness and resistance to stress-induced deformation. Although the foam mesh sleeve showed greater strain at yield, its lower elastic modulus suggests a softer structure with reduced rigidity and support capacity compared to pomelo peel. These findings highlight the mechanical advantages of pomelo peel, supporting its potential as a bioinspired material for developing sustainable and biodegradable packaging alternatives that offer enhanced protection for perishable goods.

Fig. 4B presents a comparison of the vibration resistance levels of fresh apples with and without pomelo peel wrapping. Under identical vibration conditions, as expected, apples wrapped in pomelo peel experienced lower vibrational forces than unwrapped apples. Additionally, the distribution range of vibrational forces was wider for unwrapped apples, indicating that they were more susceptible to mechanical damage. Following prolonged vibration exposure, the surface of apples wrapped in pomelo peel remained intact, whereas the unwrapped apples showed severe tissue damage. The surface area of damaged unwrapped apples exceeded 95 %, with visible juice leakage from the affected areas. These findings demonstrate that pomelo peel wrapping provided substantial protection for apples, mitigating physical impact and reducing the extent of mechanical damage during transportation. The reduced vibrational force experienced by wrapped apples can be attributed to the mesocarp's ability to uniformly absorb and distribute impact forces. Similar results were reported in a study on sustainable pomegranate packaging, where unwrapped pomegranates exhibited comparable vulnerability to mechanical damage (Mukama

Table 3
The ability of fresh apples wrapped in the peel of the red pomelo to resist falling damage.

Apple package situation	Mass /g	Fall height with damage /m	Instantaneous velocity / m s^{-1}	Impact momentum/ kg m s^{-1}	Maximum impact force /N
Wrapped in pomelo peel	504.66 ± 7.13[a]	3.2 ± 0.14[a]	7.92 ± 0.17[a]	3.96 ± 0.09[a]	4.90 ± 0.00[a]
Unwrapped	236.93 ± 5.27[b]	0.11 ± 0.02[b]	1.51 ± 0.11[b]	0.34 ± 0.02[b]	2.25 ± 0.00[b]

Note: Different lowercase letters indicate significance, the significance level is 0.05.

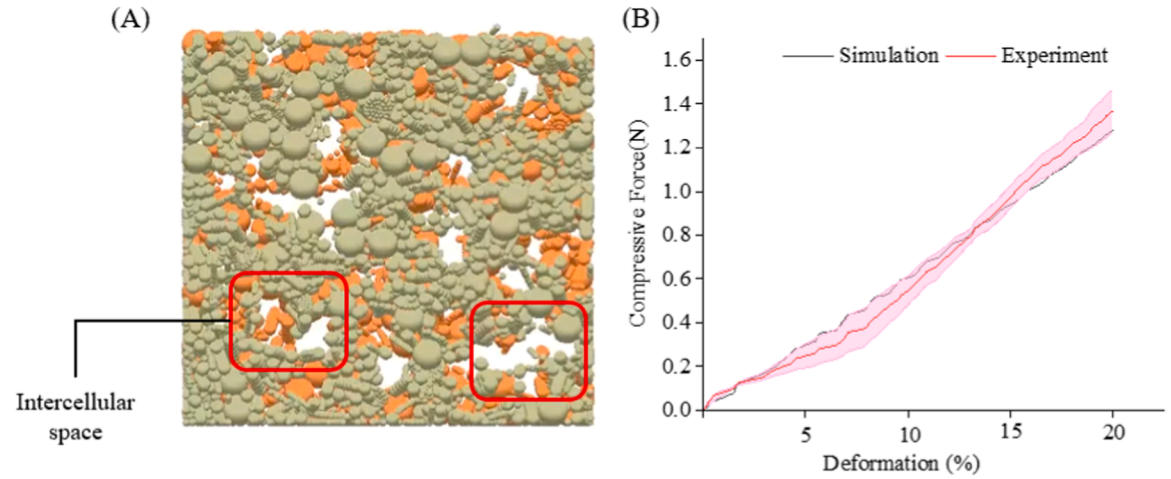

Fig. 5. Compression resistance of the pomelo mesocarp discrete element model. (A): Discrete element model of the pomelo mesocarp block; (B): Compression force-deformation percentage curves from both experimental data and model simulation. The pink-shaded area represents the B-spline error band (mean ± standard deviation) of the compression force measured in three tests when the mesocarp block deformation reached 20 %.

et al., 2024).

3.4. The ability of fresh apples wrapped in the peel of the red pomelo to resist falling damage

Table 3 presents the drop impact resistance of apples wrapped in pomelo peel. The results show that apples wrapped in pomelo peel sustained significantly less damage compared to unwrapped apples during the drop test. The drop height at which damage first appeared was 3.2 ± 0.14 m for apples wrapped in pomelo peel, whereas unwrapped apples sustained damage at a significantly lower drop height of only 0.11 ± 0.02 m. This result highlights the protective effect of the pomelo peel on apples during impact events. The instantaneous velocity and impact energy recorded for apples wrapped in pomelo peel were 7.92 ± 0.17 m s^{-1} and 3.96 ± 0.09 kg m s^{-1}, respectively, while these values were significantly reduced for unwrapped apples, reaching only 1.51 ± 0.11 m s^{-1} and 0.34 ± 0.02 kg m s^{-1}, respectively. Regarding maximum impact force, apples wrapped in pomelo peel experienced a force of 4.90 ± 0.00 N, compared to 2.25 ± 0.00 N for unwrapped apples. The increased instantaneous velocity and impact energy observed in wrapped apples can be attributed to their greater mass, resulting from the additional weight of the pomelo peel. A study by Li et al. (2023b) reported that when Fuji apples were dropped from a height of 0.2 m onto a steel substrate, the resulting bruise area was approximately 275 mm^2, and the bruise size increased as the drop height increased. Similarly, in static compression tests, Liu et al. (2022) found that Fuji apples subjected to a 2.3 mm downward compression after initial contact with a compression plate experienced elastic deformation without sustaining any damage. According to Słupska et al. (2021), a 3 mm thick polyethylene foam layer effectively protected apples from bruising when dropped from a height of 50 mm. The soft tissue structure of the pomelo mesocarp resembles foam material, demonstrating excellent energy absorption properties that help disperse impact energy during falls.

3.5. Verification of accuracy of discrete element model of fruit peel tissue block in 'Red honey' pomelo

Fig. 5A presents the established structural model of the pomelo mesocarp, demonstrating the individual cells and intercellular pore structures in the pomelo mesocarp model are distinctly defined, effectively representing the structural characteristics of the pomelo mesocarp. The red box highlights prominent pore structures within the model material. The simulated compression force-deformation results for the mesocarp tissue block, alongside the corresponding experimental data, are shown in Fig. 5B. The percentage deformation of the mesocarp tissue block is defined as the ratio of the upper plate's downward displacement to the initial height of the pomelo mesocarp discrete element model, expressed as a percentage. As shown in Fig. 5B, both the simulated compression force in the discrete element model and the measured force in the experimental compression test exhibited a similar trend, increasing gradually and non-linearly with increasing percentage deformation. The simulated compression force curve closely aligned with the experimental data range (represented by the shaded pink region), with the upper plate compression force increasing from 0 N to 1.37 N. This consistency between the simulation and experimental results validates the reliability of the established pomelo mesocarp discrete element model shown in Fig. 5A. Consequently, this validated discrete element model can be effectively employed to predict the impact resistance of real pomelo mesocarp tissue. This aligns with findings reported by Li et al. (2023a), who successfully developed a tomato mesocarp tissue block model using a discrete element method based on tomato cell dimensions, which accurately predicted the relationship between mesocarp elastic modulus and cell turgor pressure.

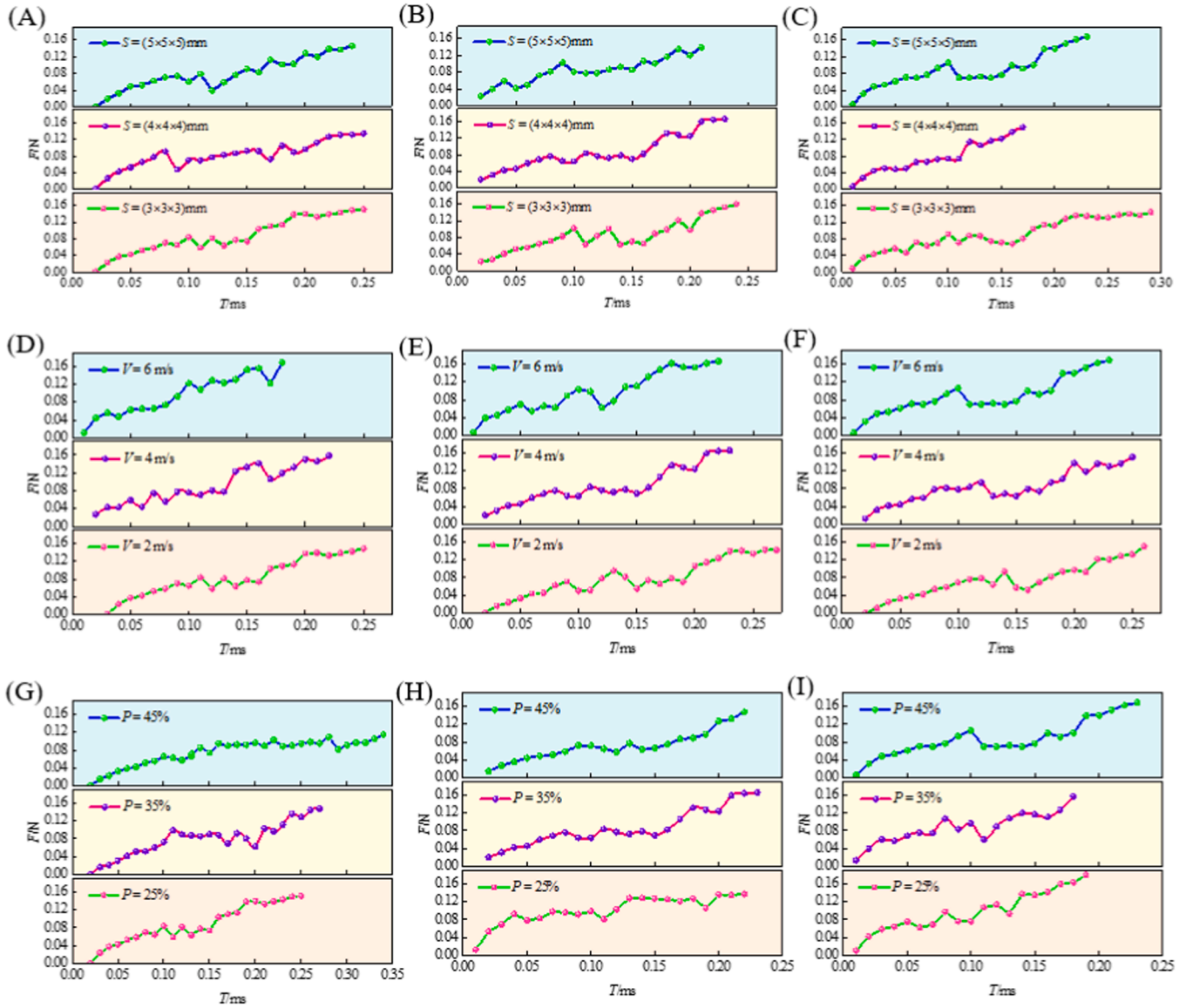

Fig. 6. Impact resistance of the pomelo mesocarp model blocks; *S* represents the model block size, *V* denotes the loading velocity, and *P* indicates the porosity; The horizontal axis shows the time (*T*) corresponding to the maximum impact force experienced by the model block. (A-C): Impact resistance of model blocks with varying sizes under porosity and loading velocity conditions of 25 % and 2 m s^{-1}, 35 % and 4 m s^{-1}, and 45 % and 6 m s^{-1}, respectively; (D-F): Impact resistance of model blocks with varying loading velocity under porosity and size conditions of 25 % and 3 mm^3, 35 % and 4 mm^3, and 45 % and 5 mm^3 , respectively; (G-I): Impact resistance of model blocks with varying porosities under loading velocity and size conditions of 2 m s^{-1} and 3 mm^3 , 4 m s^{-1} and 4 mm^3, and 6 m s^{-1} and 5 mm^3, respectively.

3.6. Impact resistance analysis of fruit peel tissue block with discrete element model

3.6.1. Effects of porosity, loading velocity and size on the damage resistance of tissue block models

Fig. 6 presents the impact resistance analysis of the pomelo mesocarp tissue block models. As shown in Fig. 6A, when the porosity and loading velocity were set at 25 % and 2 m s^{-1}, respectively, the maximum impact force and corresponding time for tissue block size with dimensions of 3 mm^3 , 4 mm^3 , and 5 mm^3 were 0.13 N and 0.25 ms, respectively. Notably, the time interval from the moment of initial force application to peak force did not exhibit significant differences among the three sizes. As illustrated in Fig. 6B, when the porosity and loading velocity were increased to 35 % and 4 m s^{-1}, respectively, the maximum impact force for models of different block sizes followed a similar trend to that observed in Fig. 6A. However, as depicted in Fig. 6C, this trend changed when the porosity and loading velocity were increased to 45 % and 6 m s^{-1}, respectively. Specifically, the tissue block model with a size of 4 mm^3 exhibited a shorter time interval from force application to peak force. This deviation may be attributed to the random arrangement of particles during model generation, where a higher concentration of solid particles localized at the central region increased the material's local density, resulting in a more compact internal structure and consequently a shorter time interval.

Fig. 6D shows that when the porosity and block size were set at 25 % and 3 mm^3, respectively, the time intervals for tissue blocks subjected to loading velocity of 2 m s^{-1}, 4 m s^{-1}, and 6 m s^{-1} varied significantly, with considerable differences between them. Fig. 6E (porosity 35 %, block size 4 mm^3) and Fig. 6F (porosity 45 %, block size 6 mm^3) both exhibit trends consistent with Fig. 6A, indicating that when porosity and block size remain constant, loading velocity has a significant influence on impact resistance. Higher loading velocity resulted in shorter time intervals from force application to peak force, demonstrating that faster loading velocity enhanced the material's resistance to impact damage.

Table 4
Response surface test scheme and results.

No.	S /mm^3	P /%	V / m s^{-1}	Y /ms
1	3	35	2	0.2501
2	4	35	4	0.21
3	3	35	6	0.19
4	3	45	4	0.28
5	5	35	6	0.17
6	5	25	4	0.2001
7	4	35	4	0.2001
8	3	25	4	0.2001
9	4	35	4	0.19
10	4	35	4	0.2
11	4	45	6	0.1599
12	4	35	4	0.19
13	5	45	4	0.2301
14	4	25	6	0.17
15	5	35	2	0.2301
16	4	45	2	0.2501
17	4	25	2	0.2301

Note: *S, P, V*, and *Y* in the table indicate tissue block size, porosity, loading velocity, and damage resistance, respectively.

Fig. 6G shows that when the loading velocity and block size were set at 2 m s^{-1} and 3 mm^3, respectively, models with porosities of 25 %, 35 %, and 45 % displayed notable differences in their respective time intervals. Fig. 6H (loading velocity 4 m s^{-1}, block size 4 mm^3) and Fig. 6I (loading velocity 6 m s^{-1}, block size 5 mm^3) reveal similar trends, reinforcing the observation that when loading velocity and block size are fixed, porosity significantly affects impact resistance. Models with lower porosity exhibited shorter time intervals from force application to peak force, indicating stronger resistance to damage. In contrast, higher porosity weakened the material's overall strength, significantly reducing its load-bearing capacity. This reduction is attributed to decreased particle contact and increased stress concentration effects at higher porosity levels, as reported by (Li et al., 2019). These results indicate that a faster loading velocity corresponds to shorter time intervals to peak force, reflecting an improved impact resistance. Additionally, lower-porosity models demonstrated superior resistance to impact damage, whereas higher porosity compromised materials strength by reducing their structural integrity and increasing susceptibility to stress concentration effects.

3.6.2. *Prediction of damage resistance of pomelo pericarp*

The pomelo pericarp model in Section 3.5 was used to establish a mathematical model to predict the damage resistance of real pomelo pericarp. The experimental design and results of this model are presented in Table 4. A multiple regression analysis was conducted using Design-Expert software, resulting in the following predictive regression equation: $Y = 0.43639–0.01590\,S + (2.82E\text{-}004)\,P + (9.2825E\text{-}003)\,V - (1.2475E\text{-}003)\,SP + (1.56676E\text{-}018)\,SV - (3.7625E\text{-}004)\,PV + 0.01854\,S^2 + (1.1015E\text{-}004)\,P^2 - (1.6275E\text{-}003)\,V^2$, in the equation, *S, V* and *P* respectively represent the block size (*S*), loading velocity (*V*) and porosity (*P*). The analysis of variance (ANOVA) results (Table 5) indicated that the model was statistically significant ($P < 0.05$) with an insignificant lack-of-fit term ($P > 0.05$), confirming the model's validity. The coefficient of determination ($R^2 = 0.9003$) showed that the model explained 90.03 % of the variance, demonstrating a strong fit and high reliability. Thus, this regression model effectively predicts the impact resistance of the simulated tissue block. Based on the F-value comparisons in Table 5, the relative influence of the factors on impact resistance was determined to follow the order: loading velocity (*V*) > porosity (*P*) > block size (*S*). Using the predictive equation, the calculated impact resistance of the tissue block model was 0.1766 ms, while the experimentally measured value was 0.1700 ms, yielding a relative error of 3.88 %. The close agreement between the predicted and actual values further supports the model's strong predictive capability. These findings align with the study by Zhang et al. (2019), which employed finite element modeling to construct a multilayer honeycomb structure based on the microstructure of pomelo peel. Their results showed that the multilayer honeycomb structure exhibited 2.5 times higher resistance to compressive stress compared to a conventional honeycomb structure. This consistency reinforces the crucial role of microstructural characteristics in cushioning performance. The established mathematical model offers valuable insights for developing bio-inspired pomelo peel packaging materials for practical applications. To further improve prediction accuracy, future studies could consider incorporating additional microstructural parameters such as cell wall thickness, pore morphology, and heterogeneity of porosity.

4. Conclusion

This study revealed that the impact resistance of pomelo peel is closely related to its thickness and microstructure. The peel thickness of 'Shatian' pomelo and 'Red honey' pomelo was measured at 9.55 mm and 3.97 mm, respectively. Under identical impact conditions, the corresponding impact forces experienced by the peels were 104.87 N and 116.53 N, with corresponding strains of 0.76 and 0.66, respectively. The dense outer epidermis and porous, reticulated mesocarp of the 'Red Honey' pomelo peel work synergistically to provide both stiffness and energy dissipation. Despite its relatively thin profile, the peel demonstrates superior impact tolerance and a higher elastic modulus,

Table 5
Analysis of variance and significance test of regression equation.

Source	Sum of squares	df	Mean square	*F* value	*p*-value	Significance
Model	0.015	9	1.662E−003	7.02	0.0088	significant
S	1.010E−003	1	1.010E−003	4.27	0.0776	
P	1.794E−003	1	1.794E−003	7.58	0.0283	*
V	9.146E−003	1	9.146E−003	38.66	0.0004	**
SP	6.225E−004	1	6.225E−004	2.63	0.1488	
SV	0.000	1	0.000	0.000	1.0000	
PV	2.265E−004	1	2.265E−004	0.96	0.3604	
S^2	1.447E−003	1	1.447E−003	6.12	0.0426	*
P^2	5.109E−004	1	5.109E−004	2.16	0.1851	
V^2	1.784E−004	1	1.784E−004	0.75	0.4139	
Residual	1.656E−003	7	2.366E−004			
Lack of fit	1.376E−003	3	4.585E−004	6.54	0.0506	
Pure error	2.804E−004	4	7.010E−005			
Cor total	0.017	16				
R^2= 0.9003						
$Y_{\text{prediction}}$ = 0.1766; Y_{actual}= 0.1700						

Note: *S, P, V*, and *Y* in the table indicate tissue block size, porosity, loading velocity, and damage resistance, respectively. Asterisks denote statistical significance of the differences (* = $P < 0.05$, ** = $P < 0.01$).

indicating that its protective performance is primarily dictated by internal architecture rather than bulk. This structure–function synergy highlights the peel's potential as a lightweight, deformable, and biodegradable material for next-generation bioinspired packaging solutions. The discrete element model (DEM) established to simulate the mesocarp structure (with R^2= 0.9003) demonstrated strong predictive accuracy, with pomelo peel impact resistance prediction of 0.1766 ms. The primary factors influencing the impact resistance of the mesocarp model were loading velocity (V) > porosity (P) > block size (S). Simulation results demonstrated that mesocarp cells and their porous structure could effectively deform and absorb energy during impact, further confirming that apples wrapped in pomelo peel exhibited enhanced protection during storage and transportation. Our findings inspire a multilayer cushion design that mimics the peel's hierarchical structure, combining a rigid outer layer with a porous mesocarp-like layer for synergistic load resistance and energy dissipation. Future cushioning materials can be designed by mimicking the peel's porous and deformable architecture to achieve efficient energy absorption and mechanical protection. These results may facilitate the development of stable, biodegradable, and scalable cushioning materials for fruit transportation and other sustainable packaging applications.

CRediT authorship contribution statement

Zhiguo Li: Writing – review & editing, Supervision, Resources, Project administration, Conceptualization. **Yande Liu:** Writing – review & editing. **Minggang Wang:** Writing – review & editing. **Clément Burgeon:** Writing – review & editing. **Fauconnier Marie-Laure:** Writing – review & editing. **Fideline Tchuenbou-Magaia:** Writing – review & editing, Supervision. **Wenzhi Tang:** Writing – review & editing, Methodology. **Hongli Qiang:** Writing – original draft, Investigation, Conceptualization. **Jincheng Yu:** Writing – original draft, Methodology, Investigation, Formal analysis, Data curation, Conceptualization.

Declaration of Competing Interest

The authors declare that they have no known competing financial interests or personal relationships that could have appeared to influence the work reported in this paper.

Acknowledgements

This work was supported by a National Key Research and Development Program of China (2025YFE0108600)

Data availability

Data will be made available on request.

References

Al-Dairi, M., Pathare, P. B., & Al-Yahyai, R. (2021). Chemical and nutritional quality changes of tomato during postharvest transportation and storage. *Journal of the Saudi Society of Agricultural Sciences, 20*(6), 401–408. https://doi.org/10.1016/j.jssas.2021.05.001

Al-Dairi, M., Pathare, P. B., Al-Yahyai, R., & Opara, U. L. (2022). Mechanical damage of fresh produce in postharvest transportation: Current status and future prospects. *Trends in Food Science Technology, 124*, 195–207. https://doi.org/10.1016/j.tifs.2022.04.018

An, X., Liu, H. J., Fadiji, T., Li, Z. G., & Dimitrovski, D. (2022). Prediction of the temperature sensitivity of strawberry drop damage using dynamic finite element method (Article) *Postharvest Biology And Technology, 190*, Article 111939. https://doi.org/10.1016/j.postharvbio.2022.111939.

An, X., Zhu, P. F., Li, Z. G., Fadiji, T., & Wani, A. A. (2023). Effect of expanded polyethylene (EPE) foam packing net design on the mechanical damage resistance of strawberry fruit during transportation (Article) *Food Packaging and Shelf Life, 40*, Article 101193. https://doi.org/10.1016/j.fpsl.2023.101193.

Chaiwong, S., Saengrayap, R., Rattanakaran, J., Chaithanarueang, A., Arwatchananukul, S., Aunsri, N., Tontiwattanakul, K., Jitkokkruad, K., Kitazawa, H., & Trongsatitkul, T. (2023). Natural rubber latex cushioning packaging to reduce vibration damage in guava during simulated transportation (Article) *Postharvest Biology And Technology, 199*, Article 112273. https://doi.org/10.1016/j.postharvbio.2023.112273.

Chen, J.H. (2022). Study on postharvest vibration damage characteristics of 'Hongmeiren' citrus fruit and development of anti-vibration packaging. Zhejiang University.

Chen, Y., Yang, S. J., Lovisa, S., Ambrose, C. G., McAndrews, K. M., Sugimoto, H., & Kalluri, R. (2021). Type-I collagen produced by distinct fibroblast lineages reveals specific function during embryogenesis and osteogenesis imperfecta (Article) *Nature Communications, 12*(1), 7199. https://doi.org/10.1038/s41467-021-27563-3.

Dagdelen, C., & Aday, M. S. (2021). The effect of simulated vibration frequency on the physico-mechanical and physicochemical properties of peach during transportation (Article) *LWT - Food Science and Technology, 137*, Article 110497. https://doi.org/10.1016/j.lwt.2020.110497.

Feng, Z. R., Sun, P. D., Zhao, F. Y., Li, M., & Ju, J. (2025). Advancements and challenges in biomimetic materials for food preservation: A review (Article) *Food Chemistry, 463*, Article 141119. https://doi.org/10.1016/j.foodchem.2024.141119.

Gao, J. B., Qiu, Y. H., Chen, F., Zhang, L. J., Wei, W., An, X. Y., & Zhu, Q. M. (2023). Pomelo peel derived nanocellulose as pickering stabilizers: fabrication of pickering emulsions and their potential as sustained-release delivery systems for lycopene (Article) *Food Chemistry, 415*, Article 135742. https://doi.org/10.1016/j.foodchem.2023.135742.

Garbowski, T., Gajewski, T., & Grabski, J. K. (2021). Estimation of the compressive strength of corrugated cardboard boxes with various openings (Article) *Energies, 14*(1), 155. https://doi.org/10.3390/en14010155.

Gu, X., Wang, F., Guan, L., Wang, X., Cheng, Y. L., Y. L, & Wu, Y. S. (2024). Advances in the design, preparation and application of biomimetic damping materials (Article) *Giant, 19*, Article 100321. https://doi.org/10.1016/j.giant.2024.100321.

Hu, R. Z., Liu, L., Liu, E. J., Tu, J., Yao, X. H., Song, P., Zhang, D. Y., Huang, Z. H., & Chen, T. (2024). Biomimetic hierarchical composites inspired by natural pomelo peel for mechanical-damage resistance and storage of fruits (Article) *Chemical Engineering Journal, 485*, Article 149853. https://doi.org/10.1016/j.cej.2024.149853.

Jentzsch, M., Becker, S., Thielen, M., & Speck, T. (2022). Functional anatomy, impact behavior and energy dissipation of the peel of citrus × limon: A comparison of citrus × limon and citrus maxima. *Plants- Basel, 11*(7). Article 991. https://doi.10.3390/plants11070991.

Jiao, X. L., Xu, W., & Duan, L. T. (2021). Study on cold chain transportation model of fruit and vegetable fresh-keeping in low-temperature cold storage environment (Article) *Discrete Dynamics In Nature And Society, 2021*, Article 8445028. https://doi.org/10.1155/2021/8445028.

Keyhan, S., Shirzad, K., Almenar, E., & Joodaky, A. (2024). Transportation vibration effects on apple bruising. *Packaging Technology and Science, 37*(11), 1065–1071. https://doi.org/10.1002/pts.2840

Kishore, A., Mithul Aravind, S., Kumar, P., Singh, A., Kumari, K., & Kumar, N. (2024). Innovative packaging strategies for freshness and safety of food products: A review. *Packaging Technology and Science, 37*(5), 399–427. https://doi.org/10.1002/pts.2800

Lazarus, B. S., Leung, V., Luu, R. K., Wong, M. T., Ruiz-Pérez, S., Barbosa, W. T., Almeida Bezerra, W. B., Barbosa, J. D. V., & Meyers, M. A. (2023). Jackfruit: Composition, structure, and progressive collapsibility in the largest fruit on the earth for impact resistance. *Acta Biomaterialia, 166*, 430–446. https://doi.org/10.1016/j.actbio.2023.04.040

Li, D. D., Liu, Y., Fadiji, T., Li, Z. G., & Okasha, M. (2023). Analysis of the correlation between mesocarp biomechanics and its cell turgor pressure: A combined FEM-DEM investigation for irrigation-caused tomato cracking. *Journal of Texture Studies, 54*(2), 206–221. https://doi.10.1111/jtxs.12720.

Li, Y., Song, S., Huang, X., & Zhao, C. (2023). Effect of fruit weight and drop height on bruise area and contact pressure characteristics of apple during free drop test (Article) *Journal of Food Processing and Preservation, 2023*(1), Article 4828539. https://doi.org/10.1155/2023/4828539.

Li, T. T., Wang, H. Y., Huang, S. Y., Lou, C. W., & Lin, J. H. (2019). Bioinspired foam composites resembling pomelo peel: Structural design and compressive, bursting and cushioning properties. *Composites Part B: Engineering, 172*, 290–298. https://doi.org/10.1016/j.compositesb.2019.04.046

Liu, X. P., Cao, Z. T., Yang, L., Chen, H., & Zhang, Y. L. (2022). Research on damage properties of apples based on static compression combined with the finite element method (Article) *Foods, 11*(13), 1851. https://doi.org/10.3390/foods11131851.

Liu, Z. G., Li, Z. G., Yue, T. L., Diels, E., & Yang, Y. G. (2020). Differences in the cell morphology and microfracture behaviour of tomato fruit (Solanum lycopersicum L.) tissues during ripening (Article) *Postharvest Biology and Technology, 164*, Article 111182. https://doi.org/10.1016/j.postharvbio.2020.111182.

Mukama, M., Tsige, A. A., Lufu, R., & Opara, U. L. (2024). Sustainable package design for efficient pomegranate cold chain: Enhancing storage space, sea freight efficiency, material sustainability, and energy conservation (Article) *Food Packaging and Shelf Life, 46*, Article 101380. https://doi.org/10.1016/j.fpsl.2024.101380.

Pisani, S., Croce, S., Mauramati, S., Marmonti, M., Cobianchi, L., Herman, I., Dorati, R., Avanzini, M. A., Genta, I., Benazzo, M., & Conti, B. (2022). Engineered full thickness electrospun scaffold for esophageal tissue regeneration: From in vitro to in vivo approach (Article) *Pharmaceutics, 14*(2), 252. https://doi.org/10.3390/pharmaceutics14020252.

dos Santos Lima, K. T., de Matos Fonseca, J., Monteiro, A. R., & Valencia, G. A. (2024). Progress in biopolymer coatings for achieving sustainable paper and paperboard packaging for food applications: A brief review. *Packaging Technology and Science, 38*(2), 109–116. https://doi.org/10.1002/pts.2861

Schäfer, I., Mlikota, M., Schmauder, S., & Weber, U. (2020). Modelling the damping response of biomimetic foams based on pomelo fruit (Article) *Computational Materials Science, 183*, Article 109801. https://doi.org/10.1016/j.commatsci.2020.109801.

Shaikh, S. A., Li, Y. M., Ma, Z., Chandio, F. A., Tunio, M. H., Liang, Z. W., & Solangi, K. A. (2021). Discrete element method (DEM) simulation of single grouser shoe-soil interaction at varied moisture contents. *Computers and Electronics in Agriculture, 191*, Article 106538. https://doi.org/10.1016/j.compag.2021.106538

Shirzad, K., & Joodaky, A. (2023). Buckling analysis of thin plates with circular cut-outs for sustainable ventilated food packaging design (Article) *Food Packaging and Shelf Life, 40*, Article 101214. https://doi.org/10.1016/j.fpsl.2023.101214.

Słupska, M., Syguła, E., Komarnicki, P., Szulczewski, W., & Stopa, R. (2021). Simple method for apples' bruise area prediction. *Materials (Basel), 15*(1). Article 139. https://doi.10.3390/ma15010139.

Thielen, M., Speck, T., & Seidel, R. (2013). Viscoelasticity and compaction behaviour of the foam-like pomelo (Citrus maxima) peel. *Journal of Materials Science, 48*, 3469–3478. https://doi.org/10.1007/s10853-013-7137-8

Wang, X. Y., Li, X., Xue, J., Zhang, H., Wang, F., & Liu, J. S. (2022). Mechanistic understanding of the effect of zein–chlorogenic acid interaction on the properties of electrospun nanofiber films (Article) *Food Chemistry: X, 16*, Article 100454. https://doi.org/10.1016/j.fochx.2022.100454.

Xu, Y., Deng, Q., Ruan, C. Q., Xu, D., & Zeng, K. F. (2024). Application of carboxymethyl cellulose and its edible composite coating in fruit preservation. *Packaging Technology and Science, 37*(8), 781–792. https://doi.org/10.1002/pts.2822

Yang, B. S., Chen, W. H., Xin, R. L., Zhou, X. H., Meng, F. D., Chen, C. Y., Liu, Q., Li, Q., Wang, X., Xu, P., Lei, Y. F., & Xue, L. J. (2022). Strong and crack-resistant hydrogel derived from pomelo peel for highly sensitive wearable sensors (Article) *Chemical Engineering Journal, 431*(P2), Article 134094. https://doi.org/10.1016/j.cej.2021.134094.

Yang, B. S., Chen, W. H., Xin, R. L., Zhou, X. H., Tan, D., Ding, C., Wu, Y., Yin, L., Chen, C. Y., Wang, S., Yu, Z. L., Pham, J. T., Liu, S., Lei, Y. F., & Xue, L. J. (2022). Pomelo peel-inspired 3D-printed porous structure for efficient absorption of compressive strain energy. *The Journal of Bionic Engineering, 19*, 448–457. https://doi.org/10.1007/s42235-021-00145-1

Yang, P. J., Hao, J., Li, Z. G., Tchuenbou-Magaia, F., & Ni, J. H. (2024). Wind disturbance-based tomato seedlings growth control. *Biosystems Engineering, 243*, 82–92. https://doi.org/10.1016/j.biosystemseng.2024.05.007

Yu, J. C., Qiang, H. L., Shi, M. W., Li, Z. G., Fadiji, T., Wani, A., & Burgeon, C. (2025). Investigation on the protection ability of two commonly packaging methods to apples during express transportation (Article) *Food Packaging and Shelf Life, 48*, Article 101475. https://doi.org/10.1016/j.fpsl.2025.101475.

Yu, J. C., Wang, M. G., Li, Z. G., Tchuenbou-Magaia, F., Wani, A., Zhu, P. F., Fadiji, T., & Liu, Y. D. (2024). Preserving freshness:innovations for fresh-eating fruit distribution and damage prevention - A review (Article) *Food Packaging and Shelf Life, 44*, Article 101323. https://doi.org/10.1016/j.fpsl.2024.101323.

Zhang, M. S., Yang, J., Wang, Y. H., Li, Z. G., & Tchuenbou-Magaia, F. (2022). A new method for reconstructing the 3D shape of single cells in fruit (Article) *Food Research International, 162*(PA), Article 112017. https://doi.org/10.1016/j.foodres.2022.112017.

Zhang, W., Yin, S., Yu, T. X., & Xu, J. (2019). Crushing resistance and energy absorption of pomelo peel inspired hierarchical honeycomb. *International Journal of Impact Engineering, 125*, 163–172. https://doi.org/10.1016/j.ijimpeng.2018.11.014

Zhang, L. H., Zhang, M., Law, C. L., & Ma, Y. M. (2023). Effect of vibration and broken cold chain on the evolution of cell wall polysaccharides during fruit cucumber (Cucumis sativus L.) shriveling under simulated transportation (Article) *Food Packaging and Shelf Life, 38*, Article 101126. https://doi.org/10.1016/j.fpsl.2023.101126.

Zhou, L. N., Zhong, C., Liu, L., Guo, Y. P., Chen, X., & Xia, Z. (2023). Structural design and performance study of corrugated fibreboard with a laminated structure. *Postharvest Biology and Technology, 36*, 411–423. https://doi.org/10.1002/pts.2718

Zhu, M. Y., Yu, J. H., Zhang, L., & Zhu, L. (2024). Preparation of passion fruit peel extract/polydopamine/hydroxypropylmethylcellulose film and its application in banana preservation. *Packaging Technology and Science, 37*(11), 1107–1117. https://doi.org/10.1002/pts.2847